To appear in *Dynamical Systems: An International Journal*
Vol. 00, No. 00, Month 20XX, 1–25

Canard solutions in planar piecewise linear systems with three zones

S. Fernández-García[a*], M. Desroches[a], M. Krupa[a] and A. E. Teruel[b]

[a]*Inria Paris-Rocquencourt Research Centre, Domaine de Voluceau - BP 105, 78153 Le Chesnay, Cedex, France;* [b]*Departament de Matemàtiques i Informàtica. Universitat de les Illes Balears. Carretera de Valldemossa km. 7.5. 07122 Palma de Mallorca. Spain.*

(*Received 00 Month 20XX; final version received 00 Month 20XX*)

In this work, we analyze the existence and stability of canard solutions in a class of planar piecewise linear systems with three zones, using a singular perturbation theory approach. To this aim, we follow the analysis of the classical canard phenomenon in smooth planar slow-fast systems and adapt it to the piecewise-linear framework. We first prove the existence of an intersection between repelling and attracting slow manifolds, which defines a maximal canard, in a non-generic system of the class having a continuum of periodic orbits. Then, we perturb this situation and we prove the persistence of the maximal canard solution, as well as the existence of a family of canard limit cycles in this class of systems. Similarities and differences between the piecewise linear case and the smooth one are highlighted.

Keywords: piecewise linear systems; singular perturbations; canard solutions

MCS Classification: 34E17; 34E15; 37G15; 37G10

1. Introduction

In the applied dynamical systems community, there is a growing interest in the analysis of non-smooth systems. This is due to the ability of these systems to model a wide variety of phenomena [13, 28] that appear to be non-smooth (like the bouncing of a billiard ball). An interesting class within this framework is that of piecewise linear (PWL) systems. The first examples of PWL systems appeared in the seminal book of Andronov, Vitt and Khaikin [1], as a tool to analyze problems coming from engineering, for instance, the modeling of electronic, mechanical and control systems (using saturation functions, impacts, switching...). Since then, the ability of PWL systems to reproduce, inter alia, the behavior of electronic circuits, has been solidly demonstrated (Chua's circuit [37], Colpitts's oscillator [29], Wien-Bridge oscillator [24, 30]). Most importantly, PWL systems are known to reproduce all aspects of nonlinear dynamics, and the fact that one has access to explicit solutions in every linearity zone, makes it possible to describe explicitly some basic elements of the dynamics and geometry of the considered systems. However, it is neither possible to obtain a general solution nor to apply classical smooth dynamical systems theory, which creates a need for a new theory specific to PWL systems. Moreover, it has been observed that PWL systems can show new behaviors, impossible to obtain under differentiability hypothesis; for instance, the fact that the matching of two stable linear systems can produce unstable dynamics [8].

*Corresponding author. Email: soledad.fernandez-garcia@inria.fr

In this article, we focus on the canard phenomenon in PWL systems. Canards occur in systems with multiple time scales. The associated phenomenon, termed *canard explosion* [5], manifests itself as a very rapid transition, upon parameter variation, from small cycles stemming from a Hopf bifurcation to relaxation oscillations, which are large-amplitude limit cycles formed by alternating slow and fast segments. The transition occurs through a family of cycles, whose characteristic feature is that they contain *canard segments*, i.e. orbit segments remaining close to an unstable slow manifold for $O(1)$ period on the fast time scale. The canard phenomenon was first reported by Benoît *et al.* in [3] in the context of the Van der Pol system with constant forcing. The limit cycles corresponding to the explosion were termed *canard cycles*. Following the work presented in [3], the canard phenomenon has been studied by many authors, using different approaches [12, 14, 25, 26]. For the sake of completeness, we give a more detailed introduction in Section 2.

Although canards have already been investigated in the context of PWL systems, there remain a number of unanswered questions; in particular, a complete theory for PWL slow-fast systems in the canard regime has not yet been fully developed. The goal of this paper is to contribute to the foundations of such a theory, by analyzing the canard phenomenon in PWL systems from the slow-fast viewpoint, that is, using tools from singular perturbation theory and establishing a parallel between the smooth and PWL frameworks for canards. The application side is important too, as canards have been shown over the years to appear in many contexts, in particular, in models of neurons. Besides, the rationale behind most neuron models is the assumption that neurons behave, in first approximation, as electronic circuits [17, 32] and PWL systems have been extensively used to model electronic circuits. On the other hand, neuron models are characterized by different time scales, and canard phenomena have been found and studied in many smooth neuron models [6, 22, 27, 31]. This provides additional motivation to further develop PWL models of neurons and, more generally, of excitable cells.

Early studies on "PWL canards" date back to the 1990's, when the existence of limit cycles with canard-like behavior was observed in [2, 23]. Specifically, a PWL version of the Van der Pol system with three zones was considered in [23], where the cubic fast nullcline of the smooth model was replaced by the graph of a PWL function with two corners, which approximate the fold points of the cubic. Numerical evidence was given that the transition between small and large limit cycles is very fast. Cycles similar to the small Van der Pol canards (*without head*) were found, but not the equivalent to the large canards (*with head*). In [2], a modification of the previous model was considered. Namely, the PWL function approximating the cubic from the Van der Pol system was taken to have four segments instead of three. The added segment was very short, almost horizontal and centered at one corner point of the previous PWL fast nullcline. Using a mix of numerical and analytical arguments, the authors could justify the existence of both small and large canards in their model, that is, cycles that stay close for some time to the central (repelling) part of the PWL fast nullcline. However, no estimation of the size of the explosion (in terms of parameter variation) was given. This was done more recently [9], in the context of the three-zone system from [23], together with the proof that there is no repelling slow manifold in the middle zone, which was given as one of the reasons for the absence of canards with head in 3-zone systems. Due to this fact, the corresponding small canard-like cycles were termed *quasi-canards* given that they still lie in parameter space along an explosive solution branch. Among the recent studies on this topic, there is also a detailed numerical exploration of a 4-zone PWL version of the FitzHugh-Nagumo system carried out in [36], building on the work of [2].

In the present work, we study a system with three zones, intended as a canonical PWL model of transition through canards without head up to the maximal canard. That is, we only consider the PWL approximation of a Van der Pol type system near one of the folds of the cubic nullcline. Our system can be seen as a zoom of the models studied in [2, 36] onto the region of generation of the canard family. Therefore, we consider one zone with an attracting slow manifold, one zone with a repelling slow manifold, and a small central zone allowing the passage of solutions from an attracting to repelling slow manifold, that is, canard solutions. We analyze this canard transition by first proving the existence of a maximal canard, which corresponds to a connection between an attracting and a repelling slow manifold, by means of the Implicit Function Theorem. Subsequently, we investigate how this connection breaks up upon an exponentially small parameter variation and we show that a family of canards without head is defined by the same equation up to exponentially small terms. This generation mechanism of canards and its dependence on the slow-fast structures and on the presence of a transition region, has not been fully presented in previous studies. In addition, our paper provides the first rigorous results on canards in the configuration including a nearly horizontal fast nullcline in the middle zone. In our presentation, we invoke standard singular perturbation techniques in order to allow for a full comparison with the smooth case. We point out similarities and differences between our results and the results in the smooth case [3, 25, 26].

The paper is organized as follows. In Section 2, we give a short overview of canard explosion in the smooth case. In Section 3, we introduce the class of systems we aim to study. In Section 4, we present the main results of the article, whose proofs are given in Section 5. Finally, Section 6 is devoted to conclusions and possible extensions of the present work.

2. Background on canard explosion in the context of smooth systems

We first review the basic ingredients of the canard phenomenon. Our presentation is based on [25, 26]. Canards appear in planar slow-fast systems of the form

$$\begin{cases} \varepsilon\dot{x} = f(x,y,a,\varepsilon), \\ \dot{y} = g(x,y,a,\varepsilon), \end{cases}$$

or equivalently (as long as $\varepsilon \neq 0$, after a time rescaling of factor $1/\varepsilon$)

$$\begin{cases} x' = f(x,y,a,\varepsilon), \\ y' = \varepsilon g(x,y,a,\varepsilon), \end{cases}$$

with $f, g \in \mathcal{C}^k, k \geq 3, a \in \mathbb{R}, 0 < \varepsilon \ll 1$. The main geometric condition is that the fast nullcline

$$S = \{(x,y) : f(x,y,a,0) = 0\},$$

also referred to as the *critical manifold*, has a fold point (x_0, y_0) for $a = a^*$ such that $g(x_0, y_0, a^*, 0) = 0$. Without loss of generality, we can assume that this point is at the origin and that $a^* = 0$. Such a *fold point*, where an additional condition on g is satisfied, is called a *canard point*. For $\varepsilon \neq 0$, the two time parametrizations written above are equivalent; however, they do not give the same limit for $\varepsilon = 0$. Indeed, one obtains an approximation of the overall slow dynamics called *slow subsystem* in the case of the first time parametrization, and an approximation of the overall fast dynamics called *fast subsystem* in the case of the second time parametrization. Canard points are defined in the singular limit $\varepsilon = 0$ as turning points of the fast subsystem. A fold point of the critical manifold divides it locally into two parts: an attracting branch S_a and a repelling branch S_r with respect to the flow of the fast subsystem. Away from the singular limit, for sufficiently small positive ε, these two invariant manifolds of the fast subsystem persist as locally invariant slow manifolds S_a^ε and S_r^ε [16]. Fenichel (slow) manifolds are well defined only up to fold points, since the normally hyperbolicity of the unperturbed manifold, that is, the critical manifold, fails at these points. However, Fenichel manifolds are overflowing and can be extended by the flow. They behave differently near a generic fold point and near a canard point.

Around a generic fold point, an attracting Fenichel slow manifold S_a^ε may follow closely the attracting branch S_a, pass in the vicinity of the fold point, and continue following approximately the fast dynamics, giving rise to the possibility of relaxation oscillations. In Fig. 1, the left fold point of the cubic curve is a generic fold point. On the other hand, around a canard point, the condition $g(0, 0, 0, 0) = 0$ combined with the non-degeneracy condition $g_x(0, 0, 0, 0) \neq 0$ (which means that the critical manifold has a non-degenerate quadratic fold) implies that there exists a solution of the slow subsystem (in the limit $\varepsilon = 0$) which passes from S_a to S_r. In this case, an attracting Fenichel slow manifold S_a^ε may follow closely the attracting branch S_a, pass in the vicinity of the fold point, and then continue to follow closely the repelling branch S_r. This suggests the existence of solution of the original system, for $0 < \varepsilon \ll 1$, containing canard segments. In Fig. 1, the right fold of the cubic is a canard point.

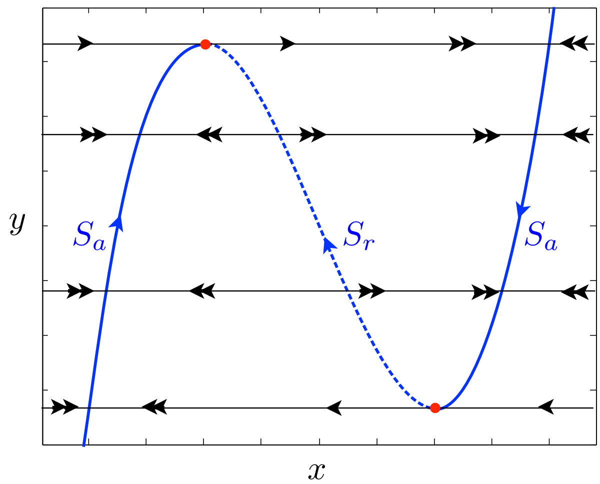

Figure 1. Cubic critical manifold with a generic fold point (left one) and a canard point (right one).

Note that slow manifolds are typically non-unique, but they are exponentially close to one another so that suitable choices can be made, according to the context. This enables to study the respective positions of attracting and repelling slow manifolds and to show the existence of canards. Indeed, the presence of exponentially small terms in ε-expansions of the slow manifolds implies that their respective position can change upon an exponentially small parameter variation. When S_a^ε is closer to the critical manifold than S_r^ε in the repelling region, this forces the existence of canards without head. For similar reasons, when S_r^ε is closer to the critical manifold than S_a^ε in the repelling region, canards with head can exist. The transition from one type of canards to the other occurs when

S_a^ε is connected to S_r^ε. This happens along a curve in the parameter plane (ε, a) and the associated canard solution is said to be a *maximal canard*. Canard cycles develop along a branch born at a Hopf bifurcation and the canard explosion takes place at a distance of $O(\varepsilon)$ from the Hopf point; this means that very close to the bifurcation, before the explosion, the cycles have the characteristics of typical Hopf cycles. This Hopf bifurcation arises only for $\varepsilon > 0$ and is usually referred to as a *singular Hopf bifurcation* [4, 21].

In the Van der Pol system, the singular Hopf bifurcation occurs exactly at the fold of the critical manifold, but this situation is not generic. Indeed, by adding a dependence on y in the slow equation, one can construct canard-explosive systems where the Hopf bifurcation generically occurs at an $O(\varepsilon)$-distance from the fold point. A simple example of such a system is

$$\begin{cases} x' = -y + x^2 - x^3, \\ y' = \varepsilon(x - a + \gamma y), \end{cases} \tag{1}$$

with $a \simeq 0$, $\gamma \in \mathbb{R}$, $0 < \varepsilon \ll 1$ and where the prime denotes the derivative with respect to the time t. When $a = 0$, system (1) has a fold point at $(x, y) = (0, 0)$. Upon variation of parameter a, one can obtain small canard cycles, maximal canards, large canard cycles and relaxation oscillations; note that the criticality of the Hopf bifurcation depends on the size and sign of γ. Furthermore, system (1) allows for multi-stability and global bifurcations (homoclinic connections) that can terminate prematurely the canard explosion. In terms of applications, system (1) is very similar to the FitzHugh-Nagumo equation, which is the simplest smooth planar mathematical model of a neuron [17, 32]. The simplest smooth slow-fast dynamical system displaying canard solutions is a quadratic vector field similar to (1) but without the cubic term in the first equation and with $a = \gamma = 0$ in the second. That minimal canard system is sometimes referred to as the *singular fold* system [25], it is Hamiltonian and possesses a continuum of canard periodic orbits; we will study a PWL equivalent of the singular fold in the next section. However, canard cycles are only possible when adding a cubic term to the singular fold system.

3. Piecewise linear systems with three zones. First properties

Following the ideas (from [2]) of adding a small piece in the corner to generate canard cycles, we consider the following class of planar piecewise linear systems with three zones depending on three parameters,

$$\begin{cases} x' = y + f(x, b, \varepsilon), \\ y' = \varepsilon(a - x), \end{cases} \tag{2}$$

where

$$f(x, b, \varepsilon) = \begin{cases} x + \varepsilon, & \text{if } x \leq -\varepsilon/(1-b), \\ bx, & \text{if } -\varepsilon/(1-b) < x \leq \varepsilon/(b+1), \\ -x + \varepsilon, & \text{if } x > \varepsilon/(b+1), \end{cases}$$

with $(x, y)^T \in \mathbb{R}^2$, $0 < \varepsilon \ll 1$, $|b| < 2\sqrt{\varepsilon}$ and $a \in (-\varepsilon/(1-b), \varepsilon/(b+1))$.

Note that the nonlinearity is gathered in the first component of the vector field, and that the second component of the vector field is continuous. In these systems, the three linearity zones are separated by the straight lines $x = -\varepsilon/(1-b)$ and $x = \varepsilon/(1+b)$. Thus, we will call the left L, central C and right R zones the regions of the phase plane defined by $x < -\varepsilon/(1-b)$, $-\varepsilon/(1-b) < x < \varepsilon/(b+1)$ and $x > \varepsilon/(b+1)$, respectively. Moreover, we will sometimes use the term "exterior zones" to refer to both left and right zones. Finally, for every point $\mathbf{p} = (x_0, y_0)^T \in \mathbb{R}^2$ and parameter vector $\boldsymbol{\eta} = (a, b, \varepsilon)$, we will denote by

$$\mathbf{x}(t; \boldsymbol{\eta}, \mathbf{p}) = (x(t; \boldsymbol{\eta}, \mathbf{p}), y(t; \boldsymbol{\eta}, \mathbf{p}))^T$$

the solution of system (2) with parameters a, b, ε and initial condition $\mathbf{x}(0; \boldsymbol{\eta}, \mathbf{p}) = \mathbf{p}$. Sometimes, we use the superscripts L, C or R to refer to the zone of the system where we are computing the solution, namely, left, central or right. We can now state a few general properties of this family of systems.

System (2) possesses exactly one equilibrium point which is in central zone C, namely, $\mathbf{q}^C = (a, -ab)^T$. The topological type of the equilibrium can be easily checked and depends on parameter b. If $b = 0$, the equilibrium point $\mathbf{q}^C$ is a center. If $b < 0$, (resp. $b > 0$) it is a stable, (resp. unstable) focus. The orientation is clockwise in the three cases.

Apart from the equilibrium point $\mathbf{q}^C$, there are two other points that are not real equilibria of the system, yet influence the dynamics in a similar way that an equilibrium does. These are $\mathbf{q}^L = (a, -a-\varepsilon)$ and $\mathbf{q}^R = (a, a-\varepsilon)$. Point $\mathbf{q}^L$ (resp. $\mathbf{q}^R$), is an equilibrium point of the system of the left (resp. right) zone, but both are located in the central zone. These points are usually called virtual equilibrium points in the context of PWL systems. It is easy to compute their topological types. Point $\mathbf{q}^L$, (resp. $\mathbf{q}^R$) is an unstable (resp. stable), node; see Fig. 2.

The eigenvalues of the left zone coefficient matrix are given by

$$\lambda_s^L = \frac{1 - \sqrt{1 - 4\varepsilon}}{2} \quad \text{and} \quad \lambda_f^L = \frac{1 + \sqrt{1 - 4\varepsilon}}{2}. \tag{3}$$

It is easy to see that $\lambda_f^L > \lambda_s^L > 0$, and that

$$\lim_{\varepsilon \to 0} \lambda_s^L = 0^+ \quad \text{and} \quad \lim_{\varepsilon \to 0} \lambda_f^L = 1^-.$$

The straight lines

$$\mu_s^L \equiv y = -\frac{\varepsilon(x-a)}{\lambda_s^L} - a - \varepsilon \quad \text{and} \quad \mu_f^L \equiv y = -\frac{\varepsilon(x-a)}{\lambda_f^L} - a - \varepsilon \tag{4}$$

are the invariant spaces corresponding to the weak and the strong eigenvalue, respectively, for the virtual equilibrium point $\mathbf{q}^L$. Note that they are invariant manifolds only for the flow in the left zone. The slope of μ_f^L tends to zero as $\varepsilon \to 0$ and that the slope of μ_s^L tends to -1 as $\varepsilon \to 0$.

Consider now the eigenvalues of the right zone coefficient matrix,

$$\lambda_s^R = \frac{-1 + \sqrt{1 - 4\varepsilon}}{2} \quad \text{and} \quad \lambda_f^R = \frac{-1 - \sqrt{1 - 4\varepsilon}}{2}. \tag{5}$$

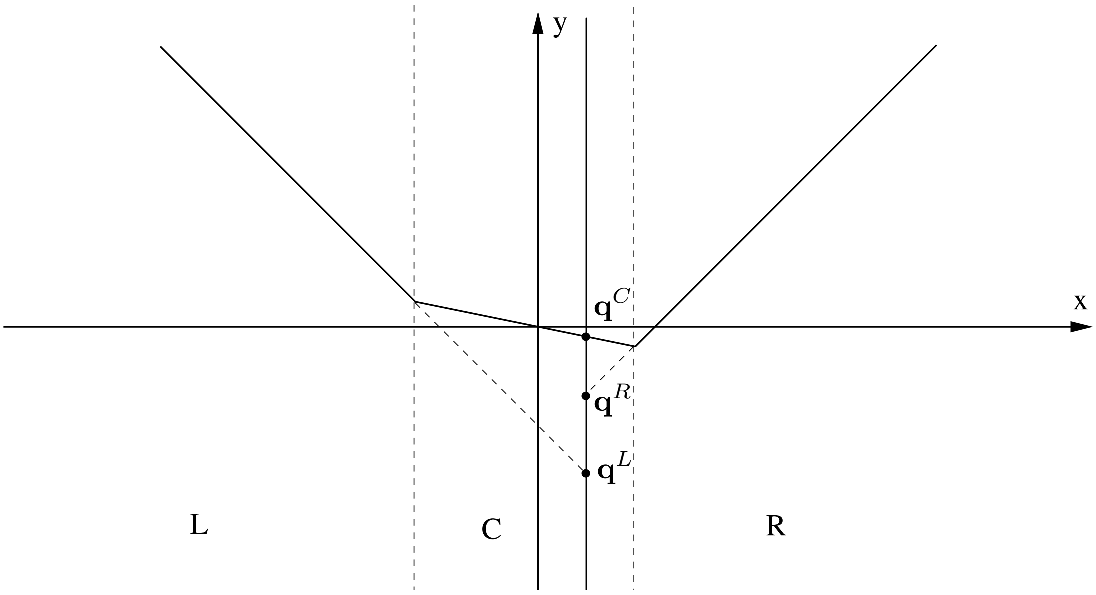

Figure 2. Zones of linearity, nullclines and equilibria (real and virtuals) of system (2).

It is easy to see that $\lambda_f^R < \lambda_s^R < 0$, and that

$$\lim_{\varepsilon\to 0} \lambda_s^R = 0^- \quad \text{and} \quad \lim_{\varepsilon\to 0} \lambda_f^R = -1^+.$$

The straight lines

$$\mu_s^R \equiv y = -\frac{\varepsilon(x-a)}{\lambda_s^R} + a - \varepsilon \quad \text{and} \quad \mu_f^R \equiv y = -\frac{\varepsilon(x-a)}{\lambda_f^R} + a - \varepsilon \tag{6}$$

are the invariant spaces corresponding to the weak and the strong eigenvalue, respectively, for the virtual equilibrium point $\mathbf{q}^R$. Note that they are invariant manifolds only for the flow in the right zone. The slope of μ_f^R tends to zero as $\varepsilon \to 0$ and the slope of μ_s^R tends to 1 as $\varepsilon \to 0$. Note that $\lambda_s^L = -\lambda_s^R$ and $\lambda_f^L = -\lambda_f^R$.

The invariant space of the right zone μ_s^R is strongly attracting and the invariant space of the left zone μ_s^L is strongly repelling. As $\varepsilon \to 0$ they approach the critical manifold of the system, namely, $y = |x|$. It follows that μ_s^R, (resp. μ_s^L) provides a canonical choice of an attracting Fenichel slow manifold S_a^ε, (resp. repelling Fenichel slow manifold S_r^ε) [15, 16, 33, 34]; see Fig. 3. Moreover, the central zone is letting the flow pass through, from the attracting manifold S_a^ε to the repelling manifold S_r^ε. Thus, the class of systems (2) possesses, in principle, all the ingredients to have canard cycles. In the following we focus on the proof of this fact.

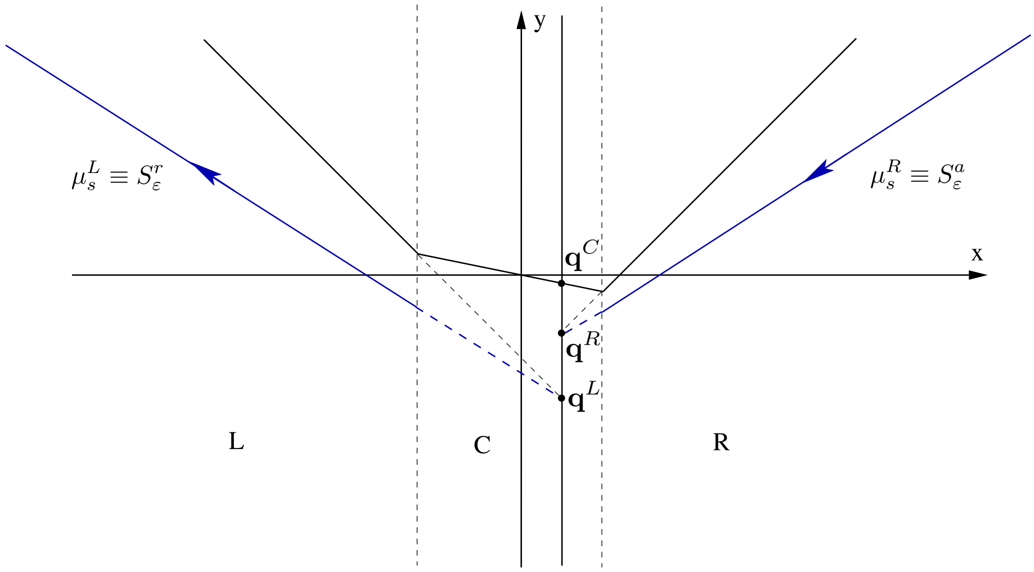

Figure 3. Zones of linearity, nullclines, equilibria (real and virtuals) of system (2) and slow manifolds corresponding to the virtual nodes of the exterior zones.

4. Main results: Maximal canard solution and family of canard cycles

In this section, we state the main results of the article. We first aim to find conditions such that the family of systems (2) possesses a maximal canard solution. To this end, we begin by analyzing the non-generic system of the family, for $a = b = 0$.

Theorem 4.1: *System (2) with $a = b = 0$ and $0 < \varepsilon \ll 1$, possesses a continuum of periodic orbits bounded below by the slow manifolds μ_s^L and μ_s^R in their corresponding zones, and by the connection from μ_s^R to μ_s^L in the central zone. Below the continuum, the orbits cross from the right zone to the central one and later to the left zone, where they escape to infinity.*

Proof. In this case, the real equilibrium is $\mathbf{q}^C = (0, 0)^T$ and it is a center. The virtual equilibria coincide $\mathbf{q}^L = \mathbf{q}^R = (0, -\varepsilon)^T$. Since, in this case, the system is time-reversible with respect to the involution $\mathcal{R}(x, y) = (-x, y)$, the conclusion follows. □

Fig. 4 shows the phase portrait of system (2) under the hypotheses of Theorem 4.1. Note that the non-generic situation described in Theorem 4.1, is analogous to that of the Hamiltonian system found in the local analysis around the canard point in the smooth case [18, 25, 26]. In this case, we find a special orbit which bounds the continuum of periodic orbits. This orbit is formed by three different parts: the slow invariant manifolds μ_s^L and μ_s^R in their corresponding zones, and their connection in the central zone. As it was previously noted, in system (2) the slow invariant manifolds μ_s^L and μ_s^R play the role of the attracting and repelling slow invariant manifolds S_r^ε and S_a^ε. Then, we can say that

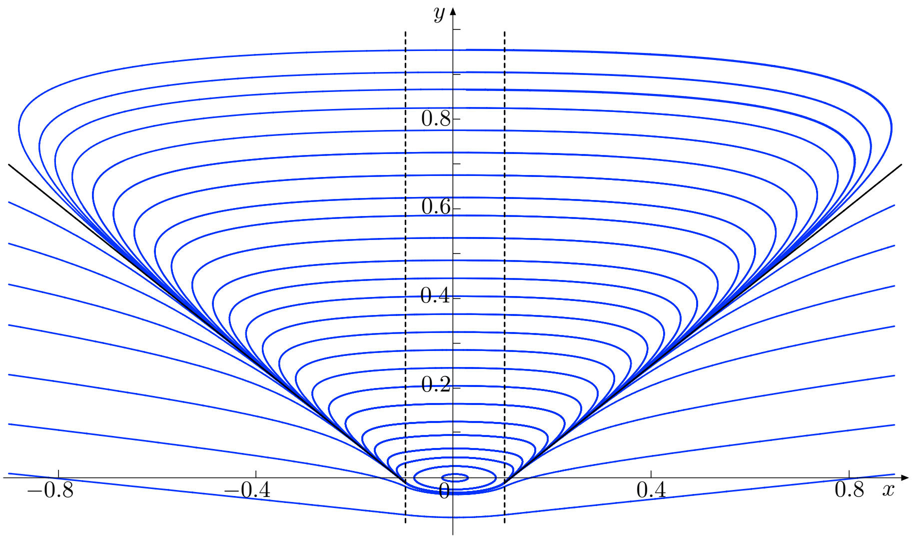

Figure 4. Phase portrait of system (2) with $a = b = 0$ and $\varepsilon = 0.1$. We also represent the slow manifolds μ_s^L and μ_s^R, and in dashed the separation lines.

this special orbit is the *maximal canard orbit* and the periodic orbits of the continuum are canard periodic orbits.

The question that naturally arises is whether, by perturbing this non-generic situation, it is possible to find appropriate values of the parameters such that the maximal canard orbit persists. In the next theorem, we state the existence of a curve in the parameter space $a = \tilde{a}(b, \varepsilon)$, such that the maximal canard remains after the perturbation.

Theorem 4.2: *There exists a function $a = \tilde{a}(b, \varepsilon)$, analytic as function of $(b, \sqrt{\varepsilon})$, defined in an open set $U \subset \mathbb{R}^2$ containing $(b, \varepsilon) = (0, 0)$, and such that, for $(b, \varepsilon) \in U \cap \{\varepsilon > 0\}$, system (2) possesses an orbit connecting the slow manifolds of the exterior zones.*

Proof. See Subsection 5.1. □

From the existence of the maximal canard solution, the existence of a family of isolated canard limit cycles in system (2) follows. This is stated in the following theorem.

Theorem 4.3: *For each point $(0, y_0)$ with $y_0 > 0$, there exists $\hat{U} \subset \mathbb{R}^2$ containing $(b, \varepsilon) = (0, 0)$, such that, for $(b, \varepsilon) \in \hat{U} \cap \{\varepsilon > 0\}$, there exists $\hat{a}(b, \varepsilon)$ with the same first terms of the Taylor series expansion as $\tilde{a}(b, \varepsilon)$ given in Theorem 4.2, such that system (2) possesses a canard limit cycle passing through $(0, y_0)$.*

Proof. See Subsection 5.2. □

Although it is not necessary to obtain an explicit approximation of the parameter function $\tilde{a}(b, \varepsilon)$ in order to prove the previous existence theorems, it becomes necessary when analyzing the stability of the canard cycles. Also, the approximation is interesting by itself, because it allows us to control the location where the canard explosion takes place. The approximation of $\tilde{a}(b, \varepsilon)$ is included in next proposition.

Proposition 4.4: *Let $\tilde{a} = \tilde{a}(b, \varepsilon)$ be the function defined in Theorem 4.2. The Taylor series expansion with respect to b around $b = 0$ is given by*

$$\tilde{a}(b, \varepsilon) = \varepsilon((\tau^*/2) - 1)b/2 + O(b^3) = \left(\frac{\pi}{4}\sqrt{\varepsilon} + O(\varepsilon)\right) b + O(b^3), \tag{7}$$

where

$$\tau^* = \frac{\pi - \sin^{-1}(2\sqrt{\varepsilon})}{\sqrt{\varepsilon}}. \tag{8}$$

Proof. See Subsection 5.3. □

The approximation of the parameter function $\tilde{a}(b,\varepsilon)$ obtained in Proposition 4.4, enables us to establish, in the next theorem, the stability of the family of canard cycles.

Theorem 4.5: *The family of canard limit cycles whose existence is stated in Theorem 4.3 is asymptotically stable if* $b > 0$ *and unstable if* $b < 0$.

Proof. See Subsection 5.4. □

Remark 4.6: Note that Theorem 4.5 implies the uniqueness of canard cycles. Indeed, if there existed two canard cycles for the same parameter values, one would have to be inside the other and the region between them would have to contain a canard cycle of opposite stability.

In Fig. 5, we represent a stable canard cycle of system (2) and two orbits in its basin of attraction. We take advantage of formula (7) to set appropriate values of the parameters such that the canard exists.

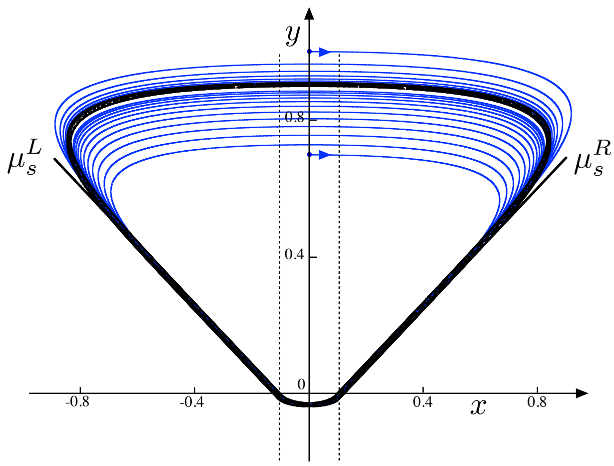

Figure 5. Phase portrait of system (2) with a stable canard cycle (thick black orbit), for $b = 0.009944$, $\varepsilon = 0.1$ and $a = \hat{a}(b,\varepsilon)$. We also represent the slow invariant manifolds μ_s^L and μ_s^R (solid black lines) and the separation lines (dashed). Two trajectories converging towards the stable canard cycles are shown (in blue), the initial condition is indicated by a dot and the direction of motion by an arrow.

Theorems 4.2 and 4.3 assert the existence of maximal canard cycles and of isolated canard limit cycles in the PWL family of systems (2). Moreover, in Theorem 4.5 the stability of such cycles is established. These results allow us so far to point out similarities and differences between canard phenomena in the PWL framework and in the classical smooth context. We find very similar features between both phenomena. In particular, if in the smooth case the limit cycles that become canards are born in a Hopf bifurcation, in the PWL case we can say that their birth takes place in a Hopf-like bifurcation [19, 20] that occurs when the real equilibrium point crosses from one of the exterior zones to the central one, by moving parameter a. In the following remark, we explain this bifurcation structure in more detail; see Fig. 6.

Remark 4.7: In this remark, we consider $b = O(\sqrt{\varepsilon})$ and $\hat{b}$ defined by $b = 2\sqrt{\varepsilon}\hat{b}$.

(1) Consider $b > 0$. A supercritical Hopf-like bifurcation takes place when the equilibrium crosses from the right to the central zone, i.e., at

$$a_H^R(b, \varepsilon) = \frac{\varepsilon}{b+1} = \frac{\varepsilon}{2\hat{b}\sqrt{\varepsilon}+1} = \varepsilon + O(\varepsilon^{3/2}) > 0.$$

Thus, as parameter a decreases through a_H^R, there appears a two-zonal stable limit cycle contained in both the central and the right zones. The amplitude of the limit cycle is growing linearly in the two zones until it crosses the left bound $x = -\varepsilon/(1-b)$ and becomes a three-zonal limit cycle. Then, the left linear system affects the dynamics and the limit cycle becomes a canard. While a decreases, the amplitude of the canard cycle is increasing until the value where the maximal canard occurs, namely,

$$\tilde{a}(b, \varepsilon) = \left(\frac{\pi}{4}\sqrt{\varepsilon} + O(\varepsilon)\right) b + O(b^3) = \frac{\pi}{2}\hat{b}\varepsilon + O(\varepsilon^{3/2}) > 0,$$

and afterwards the limit cycle disappears.

(2) Consider $b < 0$. A subcritical Hopf-like bifurcation takes place when the equilibrium crosses from the left to the central zone, i.e., at

$$a_H^L(b, \varepsilon) = -\frac{\varepsilon}{1-b} = -\frac{\varepsilon}{1-2\hat{b}\sqrt{\varepsilon}} = -\varepsilon + O(\varepsilon^{3/2}) < 0.$$

Thus, as parameter a increases through a_H^L, there appears a two-zonal unstable limit cycle contained in both the left and the central zones. The amplitude of the limit cycle is growing linearly in the two-zones until it crosses the right bound $x = \varepsilon/(1+b)$ and becomes a three-zonal limit cycle. Then, the right linear system affects the dynamics and the limit cycle becomes a canard. While a increases, the amplitude of the canard cycle is increasing until the value where the maximal canard occurs, namely,

$$\tilde{a}(b, \varepsilon) = \left(\frac{\pi}{4}\sqrt{\varepsilon} + O(\varepsilon)\right) b + O(b^3) = \frac{\pi}{2}\hat{b}\varepsilon + O(\varepsilon^{3/2}) < 0,$$

and afterwards the limit cycle disappears.

Remark 4.7 clarifies that we can reproduce, with the class of PWL systems (2), bifurcation diagrams similar to that obtained in the smooth case [25, 26]. In Fig. 6, we have represented the bifurcation diagram corresponding to the case $b > 0$.

5. Proofs of the main results

This section focuses on the proof of the results stated in Section 4. We begin with the proof of Theorem 4.2 about the existence of the maximal canard solution.

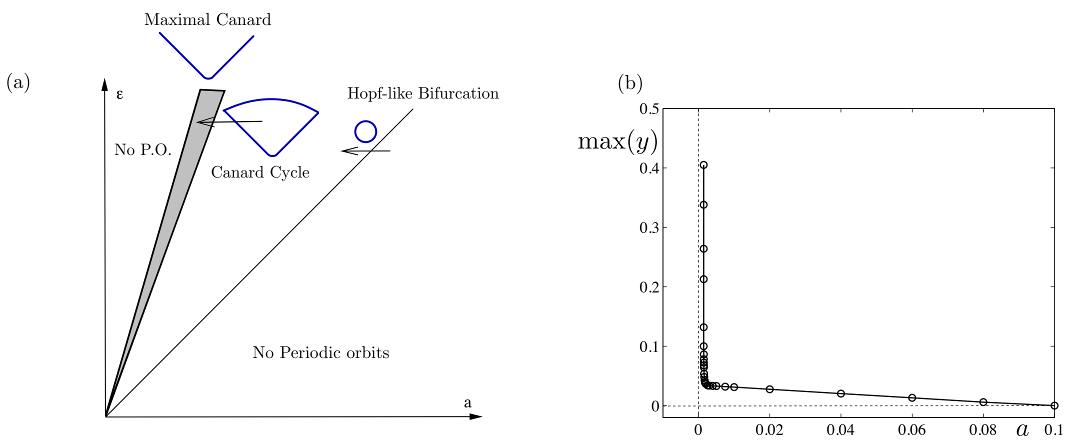

Figure 6. Panel (a) : Bifurcation diagram for $\hat{b} > 0$. Consider $\varepsilon > 0$ fixed and $a > 0$ in the rightmost sector. By decreasing a, a Hopf-like bifurcation takes place, giving rise to a small stable limit cycle. The limit cycle is growing while a decreases. When a arrives to the grey shaded region, the limit cycle becomes a canard cycle. Along the leftmost line the family of canard cycles ends at a maximal canard connection. Panel (b) : Explosive branch of limit cycles obtained by direct simulation when varying parameter a for fixed $\varepsilon = 0.1$ and $b = 0.009944$.

5.1. *Proof of Theorem 4.2*

From now on, we denote $\mathbf{p}_s^R(\boldsymbol{\eta})$, where $\boldsymbol{\eta} = (a, b, \varepsilon)$, the intersection point between the right slow manifold μ_s^R and the separation line $x = \varepsilon/(1+b)$, and $\mathbf{p}_s^L(\boldsymbol{\eta})$ the intersection point between the left slow manifold μ_s^L and the separation line $x = -\varepsilon/(1-b)$. The existence of the maximal canard solution reduces to the existence of an orbit connecting points $\mathbf{p}_s^R$ and $\mathbf{p}_s^L$ (see Fig. 7). The set of conditions characterizing this connection is given by the existence of $\tau > 0$, $0 < \varepsilon \ll 1$, $|b| < 2\sqrt{\varepsilon}$ and $a \in (-\varepsilon/(1-b), \varepsilon/(b+1))$, such that, for

$$\mathbf{p}_s^R(\boldsymbol{\eta}) = \left(\varepsilon/(1+b), a - \varepsilon - \varepsilon(\varepsilon/(1+b) - a)/\lambda_s^R\right)^T := (x_0^R, y_0^R)^T, \tag{9}$$

the following conditions hold:

$$x^C(\tau; \boldsymbol{\eta}, \mathbf{p}_s^R) = -\frac{\varepsilon}{1-b}, \tag{10}$$

$$y^C(\tau; \boldsymbol{\eta}, \mathbf{p}_s^R) = -\frac{\varepsilon}{\lambda_s^L}(x^C(\tau; \boldsymbol{\eta}, \mathbf{p}_s^R) - a) - a - \varepsilon, \tag{11}$$

$$x^C(s; \boldsymbol{\eta}, \mathbf{p}_s^R) \in \left(-\frac{\varepsilon}{1-b}, \frac{\varepsilon}{1+b}\right) \quad \text{for all} \quad s \in (0, \tau). \tag{12}$$

In a first step, we analyze the existence of solutions to the set of conditions (10)-(11), that is, the closing equations associated to the connection. We define the following functions,

$$\begin{cases} F(\tau, a, b, \varepsilon) = x^C(\tau; \boldsymbol{\eta}, \mathbf{p}_s^R) + \dfrac{\varepsilon}{1-b}, \\ G(\tau, a, b, \varepsilon) = y^C(\tau; \boldsymbol{\eta}, \mathbf{p}_s^R) + \dfrac{\varepsilon}{\lambda_s^L}(x^C(\tau; \boldsymbol{\eta}, \mathbf{p}_s^R) - a) + a + \varepsilon. \end{cases} \tag{13}$$

Thus, the solution of the closing equations is equivalent to the solution $(\tau, a, b, \varepsilon)$ of the

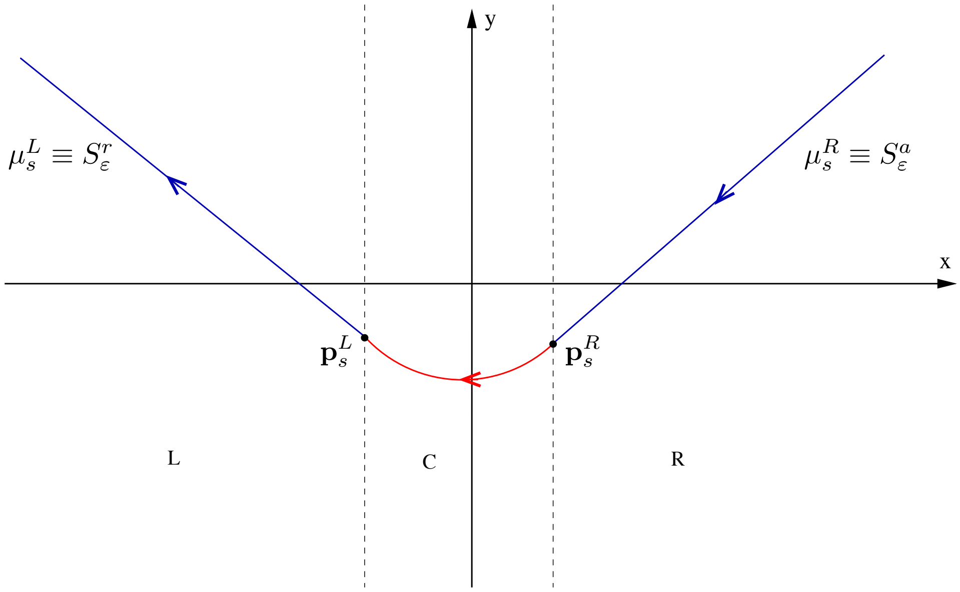

Figure 7. Representation of the possible maximal canard in system (2).

system

$$\begin{cases} F(\tau, a, b, \varepsilon) = 0, \\ G(\tau, a, b, \varepsilon) = 0. \end{cases} \tag{14}$$

Furthermore, the inequality (12) is equivalent to

$$F(s, a, b, \varepsilon) \in \left(0, \frac{\varepsilon}{1-b} + \frac{\varepsilon}{1+b}\right) \quad \text{for all} \quad s \in (0, \tau). \tag{15}$$

By integrating the linear system of the central zone with initial condition $\mathbf{p}_s^R$, we obtain the following explicit expression of the solution,

$$\begin{cases} x^C(\tau; \boldsymbol{\eta}, \mathbf{p}_s^R) & = \exp((b\tau)/2)\dfrac{ab+a-\varepsilon}{(b+1)\sqrt{4\varepsilon-b^2}} \\ & \cdot \Big((b-2\lambda_s^R)\sin(\tilde{\beta}\tau) - 2\tilde{\beta}\cos(\tilde{\beta}\tau)\Big) + a, \\ y^C(\tau; \boldsymbol{\eta}, \mathbf{p}_s^R) & = \exp((b\tau)/2)\dfrac{ab+a-\varepsilon}{(b+1)\sqrt{4\varepsilon-b^2}} \\ & \cdot \Big((b(\lambda_s^R - b) + 2\varepsilon)\sin(\tilde{\beta}\tau) + 2\tilde{\beta}(b-\lambda_s^R)\cos(\tilde{\beta}\tau)\Big) - ab, \end{cases} \tag{16}$$

where

$$\tilde{\beta}(b, \varepsilon) = \sqrt{4\varepsilon - b^2}/2.$$

After rescaling parameters as follows :

$$b = 2\hat{b}\sqrt{\varepsilon}; \quad \tau = \hat{\tau}/\sqrt{\varepsilon}; \quad a = \hat{a}\varepsilon, \tag{17}$$

we find a branch of solutions of system (14), described in the following lemma.

Lemma 5.1: *There exist an open set $U \subset \mathbb{R}^2$ containing $(\hat{b}, \varepsilon) = (0, 0)$ and two analytic functions $\bar{\tau}(\hat{b}, \varepsilon)$ and $\bar{a}(\hat{b}, \varepsilon)$ defined in U, such that $\bar{\tau}(0, 0) = \pi$, $\bar{a}(0, 0) = 0$ and when $\varepsilon > 0$*

$$(\tilde{\tau}(b, \varepsilon), \tilde{a}(b, \varepsilon), b, \varepsilon)$$

is a solution of system (14), where

$$\tilde{\tau}(b, \varepsilon) = \bar{\tau}(b/(2\sqrt{\varepsilon}), \varepsilon)/\sqrt{\varepsilon}$$

and

$$\tilde{a}(b, \varepsilon) = \bar{a}(b/(2\sqrt{\varepsilon}), \varepsilon)\varepsilon.$$

Proof. Let

$$\begin{aligned} \phi(\hat{\tau}, \hat{a}, \hat{b}, \varepsilon) &= \frac{\exp(\hat{b}\hat{\tau})(\hat{a} - 1 + 2\sqrt{\varepsilon}\hat{a}\hat{b})}{(1 + 2\sqrt{\varepsilon}\hat{b})\sqrt{1 - \hat{b}^2}}, \\ \theta(\hat{b}, \hat{\tau}) &= \hat{\tau}\sqrt{1 - \hat{b}^2}. \end{aligned} \tag{18}$$

It follows from the definition of F (see (13)) and the formula for x^C (see (16)) that $F = \varepsilon\hat{F}$, where $\hat{F}$ is given by

$$\hat{F}(\hat{\tau}, \hat{a}, \hat{b}, \varepsilon) = \phi\left(-\sqrt{1 - \hat{b}^2}\cos(\theta) + (\hat{b} + \sqrt{\varepsilon})\sin(\theta)\right) + \hat{a} + \frac{1}{1 - 2\sqrt{\varepsilon}\hat{b}} + O(\varepsilon). \tag{19}$$

For G the estimate is more involved. First, note that

$$y^C = \varepsilon^{3/2}\left(\phi((2\hat{b} + \sqrt{\varepsilon})\sqrt{1 - \hat{b}^2}\cos(\theta) + (1 - 2\hat{b}^2 + \sqrt{\varepsilon}\hat{b})\sin(\theta)) - 2\hat{a}\hat{b} + O(\varepsilon)\right).$$

Second, we re-write G as follows

$$G = y^C + \frac{\varepsilon}{\lambda_s^L}F - \frac{\varepsilon}{\lambda_s^L}\left(\frac{\varepsilon}{1 - \sqrt{\varepsilon}\hat{b}} + \varepsilon\hat{a}\right) + \varepsilon\hat{a} + \varepsilon.$$

By (3) it is clear that $\varepsilon/\lambda_s^L = 1 + O(\varepsilon)$, hence,

$$-\frac{\varepsilon}{\lambda_s^L}\left(\frac{\varepsilon}{1 - \sqrt{\varepsilon}\hat{b}} + \varepsilon\hat{a}\right) + \varepsilon\hat{a} + \varepsilon = -\frac{\varepsilon}{1 - 2\sqrt{\varepsilon}\hat{b}} + \varepsilon + O(\varepsilon^2) = -2\varepsilon^{3/2}\hat{b} + O(\varepsilon^2).$$

It now follows that $G = \varepsilon^{3/2}\hat{G} + (\varepsilon/\lambda_s^L)\hat{F}$, where $\hat{F}$ is given by (19) and

$$\hat{G}(\hat{\tau}, \hat{a}, \hat{b}, \varepsilon) = \phi\left((2\hat{b} + \sqrt{\varepsilon})\sqrt{1 - \hat{b}^2}\cos(\theta) + (1 - 2\hat{b}^2 + \sqrt{\varepsilon}\hat{b})\sin(\theta)\right) - 2\hat{a}\hat{b} - 2\hat{b} + O(\varepsilon).$$

Hence, solving $F = G = 0$ for $\varepsilon > 0$ is equivalent to solving $\hat{F} = \hat{G} = 0$. For $\varepsilon = 0$, we have

$$\begin{aligned} \hat{F} &= \frac{\exp(\hat{b}\hat{\tau})(\hat{a}-1)}{\sqrt{1-\hat{b}^2}}\left(-\sqrt{1-\hat{b}^2}\cos(\theta) + \hat{b}\sin(\theta)\right) + \hat{a} + 1, \\ \hat{G} &= \frac{\exp(\hat{b}\hat{\tau})(\hat{a}-1)}{\sqrt{1-\hat{b}^2}}\left(2\hat{b}\sqrt{1-\hat{b}^2}\cos(\theta) + (1-2\hat{b}^2)\sin(\theta)\right) - 2\hat{a}\hat{b} - 2\hat{b}. \end{aligned} \tag{20}$$

For $\hat{a} = \hat{b} = 0$, equation $\hat{F} = 0$ gives the condition $\cos(\hat{\tau}) = -1$, which yields $\hat{\tau} = \pi$. Further $\hat{G} = 0$ is satisfied for $\hat{a} = \hat{b} = 0$ and $\hat{\tau} = \pi$. To apply the Implicit Function Theorem, it is necessary to prove that $\det(J(\pi, 0, 0, 0)) \neq 0$, where

$$J(\hat{\tau}, \hat{a}, \hat{b}, \varepsilon) = \begin{pmatrix} \dfrac{\partial \hat{F}}{\partial \hat{\tau}}(\hat{\tau}, \hat{a}, \hat{b}, \varepsilon) & \dfrac{\partial \hat{F}}{\partial \hat{a}}(\hat{\tau}, \hat{a}, \hat{b}, \varepsilon) \\ \dfrac{\partial \hat{G}}{\partial \hat{\tau}}(\hat{\tau}, \hat{a}, \hat{b}, \varepsilon) & \dfrac{\partial \hat{G}}{\partial \hat{a}}(\hat{\tau}, \hat{a}, \hat{b}, \varepsilon) \end{pmatrix}. \tag{21}$$

It is easy to see that

$$\frac{\partial \hat{F}}{\partial \hat{a}}(\pi, 0, 0, 0) = 2, \quad \frac{\partial \hat{F}}{\partial \hat{\tau}}(\pi, 0, 0, 0) = 0,$$

$$\frac{\partial \hat{G}}{\partial \hat{a}}(\pi, 0, 0, 0) = 0, \quad \frac{\partial \hat{G}}{\partial \hat{\tau}}(\pi, 0, 0, 0) = 1,$$

and then, $\det(J(\pi, 0, 0, 0)) = -2 \neq 0$. Hence, the Implicit Function Theorem yields a solution defined on a neighborhood of $(0, 0)$ in the $(\hat{b}, \varepsilon)$ plane. Moreover

$$\frac{\partial \hat{F}}{\partial \hat{b}}(\pi, 0, 0, 0) = -\pi, \quad \frac{\partial \hat{G}}{\partial \hat{b}}(\pi, 0, 0, 0) = 0.$$

□

To ensure the existence of the connection, we must prove that the solutions of the closing equations (10) and (11), whose existence is guaranteed by Lemma 5.1, satisfy inequality (12), or equivalently, (15). Geometric arguments will allow us to conclude that they actually correspond to the connection between the slow manifolds of the right and left zones of system (2).

As an auxiliary result, we obtain the solution corresponding to the non-generic case presented in Theorem 4.1.

Lemma 5.2: *For $a = b = 0$ system (14) has the explicit solution*

$$\tau^* = \frac{\pi - \sin^{-1}(2\sqrt{\varepsilon})}{\sqrt{\varepsilon}},$$

with $0 < \varepsilon \ll 1$. This solution corresponds to the non-generic case presented in Theorem 4.1.

Proof. This follows from a straightforward computation. □

Finally, the next lemma finishes the proof of Theorem 4.2.

Lemma 5.3: *Functions $\tilde{\tau} = \tilde{\tau}(b, \varepsilon)$ and $\tilde{a} = \tilde{a}(b, \varepsilon)$, given in Lemma 5.1, satisfy inequality (15) for every $|b| \neq 0$, $0 < \varepsilon \ll 1$.*

Proof. We need to prove

$$F(s, \tilde{a}, b, \varepsilon) \in \left(0, \frac{\varepsilon}{1-b} + \frac{\varepsilon}{1+b}\right) \quad \text{for all} \quad s \in (0, \tilde{\tau}).$$

We proceed by contradiction. Assume that there exists $\tau_1 < \tilde{\tau}$ such that $F(\tau_1, \tilde{a}, b, \varepsilon) > \varepsilon/(1-b) + \varepsilon/(1+b)$, or equivalently, $\mathrm{x}^C(\tau_1; \tilde{\boldsymbol{\eta}}, \mathbf{p}_s^R(\tilde{\boldsymbol{\eta}})) > -\varepsilon/(1-b)$, where $\tilde{\boldsymbol{\eta}} = (\tilde{a}, b, \varepsilon)$. Then, to allow the flow to come back to the line $x = -\varepsilon/(1-b)$, it is necessary that $\tilde{\tau} \geq 2\pi/\sqrt{\varepsilon} \geq 2\tau^*$, where τ^* is given in (8) and corresponds to the solution for $a = b = 0$. But $\tilde{\tau}(0, \varepsilon) = \tau^*$, which contradicts $\tilde{\tau} \geq 2\tau^*$. An analogous reasoning allows to prove that $F(s, \tilde{a}, b, \varepsilon) > 0$ for all $s \in (0, \tilde{\tau})$. □

Therefore, the proof of the existence of a subfamily of the PWL systems (2) having a maximal canard solution, is now complete. In the following remark, we present an alternative proof of Theorem 4.2. based on the fact that system (2) is time-reversible with respect to the involution

$$\mathcal{Q}(a, b, \varepsilon, x, y) = (-a, -b, \varepsilon, -x, y). \tag{22}$$

Albeit more direct, this alternative argument is also more difficult to generalize. Moreover, following this approach it is not possible to arrive to the explicit expression of a that we obtain in Proposition 4.4 and that we use later to deal with the stability of the canard solutions.

Remark 5.4: System (2) is time-reversible with respect to the involution (22). Define the function $\sigma(a, b, \varepsilon)$ as the second component of the intersection with the line $x = a$ of the orbit with initial condition (9). Since the dynamics in the central zone is of focus type, the function σ it is always defined and is an analytical function of $\varepsilon > 0$, a and b, as the Poincaré map. Taking into account the symmetry, the condition of existence of the maximal canard reads

$$\omega(a, b, \varepsilon) := \sigma(a, b, \varepsilon) - \sigma(-a, -b, \varepsilon) = 0. \tag{23}$$

It is easy to see that $\sigma(a, b, \varepsilon) \leq -ab$. The equality arises only when the equilibrium is in the right boundary, that is $a = \varepsilon/(1+b)$. Hence,

$$\omega(-\varepsilon/(1-b), b, \varepsilon) < 0 < \omega(\varepsilon/(1+b), b, \varepsilon).$$

Note that $\sigma(a,b,\varepsilon)$ is an increasing function of a because, as a increases, the vertical nullcline is approaching the right boundary and the actual orbit arrives before and above $x=a$. Then, for each (b,ε), there exits a unique value $\tilde{a}(b,\varepsilon)$ of a satisfying (23). To prove the analyticity, consider the change (17) together with $(x,y)=(\hat{x}\varepsilon,\hat{y}\varepsilon^{3/2})$. In the new variables, σ is an analytic function of $(\hat{a},\hat{b},\varepsilon)$. To find the lowest order approximation of function σ we work with the rescaled problem for $\varepsilon=0$. A computation similar to the one used to obtain (20) yields

$$\sigma(\hat{a},\hat{b},0)=(\hat{a}-1)\exp\left(\frac{\hat{b}\arccos\hat{b}}{\sqrt{1-\hat{b}^2}}\right)-2\hat{a}\hat{b},$$

and consequently

$$\omega(\hat{a},\hat{b},0)=\exp\left(\frac{\hat{b}\arccos\hat{b}}{\sqrt{1-\hat{b}^2}}\right)\left(\hat{a}\left(1+\exp\left(\frac{-\hat{b}\pi}{\sqrt{1-\hat{b}^2}}\right)\right)-1+\exp\left(\frac{-\hat{b}\pi}{\sqrt{1-\hat{b}^2}}\right)\right).$$

The derivative of ω with respect to a is non zero, and it is possible to apply the Implicit Function Theorem, where the analyticity of $\tilde{a}(b,\sqrt{\varepsilon})$ follows.

In next subsection, we focus on the proof of Theorem 4.3. We are going to use the results of this section to establish the existence of canard cycles in the family of PWL systems (2).

5.2. *Proof of Theorem 4.3*

Consider a point $(0,y_0)$ with $y_0>0$. By integrating backwards, the orbit will cross from the central to the left zone and will reach a neighborhood of μ_s^L in an $O(\varepsilon)$ time. After that, as the manifold μ_s^L is repelling and we are integrating backwards, the orbit targets the central zone, while the distance to μ_s^L is contracting with contraction rate $O(\exp(-c/\varepsilon))$, where c is a positive constant depending on y_0, for a time interval of order one. Thus, the orbit reaches the central zone at a point $\mathbf{p}_1$ which is exponentially close to the intersection between the invariant manifold μ_s^L and the separation line $x=-\varepsilon/(1-b)$, denoted $\mathbf{p}_s^L$.

By integrating forward, the orbit will cross from the central to the right zone and will reach a neighborhood of μ_s^R in $O(\varepsilon)$ time. After that, as the manifold μ_s^R is attracting, the orbit targets the central zone, while the distance to μ_s^R is contracting with contraction rate $O(\exp(-c/\varepsilon))$, where c is a positive constant depending on y_0, for a time interval of order one. Thus, the orbit reaches the central zone at a point $\mathbf{p}_{-1}$ which is exponentially close to the intersection between the invariant manifold μ_s^R and the separation line $x=\varepsilon/(1+b)$, that is, $\mathbf{p}_s^R$ given in (9).

Regarding the connection between $\mathbf{p}_{-1}$ and $\mathbf{p}_1$, note that $\mathbf{p}_{-1}$ and $\mathbf{p}_1$ and their derivatives are exponentially close to $\mathbf{p}_s^R$ and $\mathbf{p}_s^L$ and their derivatives, respectively. It follows that the equations establishing the connection between $\mathbf{p}_{-1}$ and $\mathbf{p}_1$ has the form

$$\begin{pmatrix} F(\tau,a,b,\varepsilon) \\ G(\tau,a,b,\varepsilon) \end{pmatrix}+\boldsymbol{\xi}(y_0,a,b,\varepsilon)=\begin{pmatrix} 0 \\ 0 \end{pmatrix},$$

where F and G are the functions establishing the connection between $\mathbf{p}_s^R$ and $\mathbf{p}_s^L$ (14) given in (13), and $\boldsymbol{\xi}(y_0,a,b,\varepsilon)=(\xi_1(y_0,a,b,\varepsilon),\xi_2(y_0,a,b,\varepsilon))$ with $\xi_1(y_0,a,b,\varepsilon)$,

$\xi_2(y_0, a, b, \varepsilon)$ and their derivatives are $O(\exp(-c/\varepsilon))$ small, where c is a positive constant depending on y_0. Thus, we can apply the Implicit Function Theorem to the set of equations which establish the connection between $\mathbf{p}_{-1}$ and $\mathbf{p}_1$, as we did to equations (14).

Therefore, one obtains the existence of $\hat{U} \subset \mathbb{R}^2$ containing $(b, \varepsilon) = (0, 0)$, such that, for $(b, \varepsilon) \in \hat{U} \cap \{\varepsilon > 0\}$, there exists $\hat{a}(b, \varepsilon)$ with the same first terms of the Taylor series expansion as $\tilde{a}(b, \varepsilon)$ given in Theorem 4.2, such that system (2) possesses a canard limit cycle.This concludes the proof.

5.3. *Proof of Proposition 4.4*

We proceed by implicit differentiation. From Lemma 5.1, $(\tilde{\tau}(b, \varepsilon), \tilde{a}(b, \varepsilon), b, \varepsilon)$ is a solution of system (14), that is,

$$\begin{cases} F(\tilde{\tau}(b, \varepsilon), \tilde{a}(b, \varepsilon), b, \varepsilon) = 0, \\ G(\tilde{\tau}(b, \varepsilon), \tilde{a}(b, \varepsilon), b, \varepsilon) = 0, \end{cases} \tag{24}$$

and then, from Lemma 5.2, it satisfies $\tilde{\tau}(0, \varepsilon) = \tau^*$ and $\tilde{a}(0, \varepsilon) = 0$. Let us denote

$$\mathbf{p}^* = \mathbf{p}_s^R(0, 0, \varepsilon) = (\varepsilon, \lambda_s^R \varepsilon).$$

By taking derivatives in system (24) with respect to b at $b = 0$, it is easy to see that $\frac{\partial \tilde{\tau}}{\partial b}(0, \varepsilon)$ and $\frac{\partial \tilde{a}}{\partial b}(0, \varepsilon)$ must satisfy the system of equations

$$\begin{pmatrix} \dfrac{\partial F}{\partial \tau}(\tau^*, 0, 0, \varepsilon) & \dfrac{\partial F}{\partial a}(\tau^*, 0, 0, \varepsilon) \\ \dfrac{\partial G}{\partial \tau}(\tau^*, 0, 0, \varepsilon) & \dfrac{\partial G}{\partial a}(\tau^*, 0, 0, \varepsilon) \end{pmatrix} \begin{pmatrix} \dfrac{\partial \tilde{\tau}}{\partial b}(0, \varepsilon) \\ \dfrac{\partial \tilde{a}}{\partial b}(0, \varepsilon) \end{pmatrix} = - \begin{pmatrix} \dfrac{\partial F}{\partial b}(\tau^*, 0, 0, \varepsilon) \\ \dfrac{\partial G}{\partial b}(\tau^*, 0, 0, \varepsilon) \end{pmatrix}. \tag{25}$$

Let us begin with the computation of $\frac{\partial G}{\partial \tau}(\tau, a, b, \varepsilon)$. From the definition of function G, (see (13))

$$\frac{\partial G}{\partial \tau}(\tau, a, b, \varepsilon) = \frac{\partial y^C}{\partial \tau}(\tau; \boldsymbol{\eta}, \mathbf{p}_s^R) + \frac{\varepsilon}{\lambda_s^L} \left(\frac{\partial x^C}{\partial \tau}(\tau; \boldsymbol{\eta}, \mathbf{p}_s^R) \right). \tag{26}$$

From system (2), in the central zone $\dot{x} = y + bx$, $\dot{y} = \varepsilon(a - x)$, and then,

$$\frac{\partial G}{\partial \tau}(\tau, a, b, \varepsilon) = \varepsilon(a - x^C(\tau; \boldsymbol{\eta}, \mathbf{p}_s^R)) + \frac{\varepsilon}{\lambda_s^L} \left(y^C(\tau; \boldsymbol{\eta}, \mathbf{p}_s^R) + b x^C(\tau; \boldsymbol{\eta}, \mathbf{p}_s^R) \right). \tag{27}$$

Now, it follows from $x^C(\tau^*; \mathbf{0}, \mathbf{p}^*) = -\varepsilon$, $y^C(\tau^*; \mathbf{0}, \mathbf{p}^*) = \lambda_s^R \varepsilon$, and expression (27) that

$$\frac{\partial G}{\partial \tau}(\tau^*, 0, 0, \varepsilon) = 0.$$

The computation of $\frac{\partial F}{\partial \tau}(\tau, a, b, \varepsilon)$ is similar to $\frac{\partial G}{\partial \tau}(\tau, a, b, \varepsilon)$,

$$\frac{\partial F}{\partial \tau}(\tau, a, b, \varepsilon) = \frac{\partial x^C}{\partial \tau}(\tau; \boldsymbol{\eta}, \mathbf{p}_s^R) = y^C(\tau; \boldsymbol{\eta}, \mathbf{p}_s^R) + b x^C(\tau; \boldsymbol{\eta}, \mathbf{p}_s^R), \tag{28}$$

and then,

$$\frac{\partial F}{\partial \tau}(\tau^*,0,0,\varepsilon) = y^C(\tau^*;\mathbf{0},\mathbf{p}^*) = \lambda_s^R \varepsilon.$$

Now, we obtain $\frac{\partial G}{\partial a}(\tau,a,b,\varepsilon)$. From definition (13),

$$\frac{\partial G}{\partial a}(\tau,a,b,\varepsilon) = \frac{\partial y^C}{\partial a}(\tau;\boldsymbol{\eta},\mathbf{p}_s^R) + \frac{\varepsilon}{\lambda_s^L}\left(\frac{\partial x^C}{\partial a}(\tau;\boldsymbol{\eta},\mathbf{p}_s^R) - 1\right) + 1. \tag{29}$$

From the explicit expression of the solution in the central zone given in (16), it is not difficult to arrive at

$$\begin{aligned} \frac{\partial x^C}{\partial a}(\tau^*;\mathbf{0},\mathbf{p}^*) &= 2, \\ \frac{\partial y^C}{\partial a}(\tau^*;\mathbf{0},\mathbf{p}^*) &= 2\lambda_2^R, \end{aligned} \tag{30}$$

from which we get

$$\frac{\partial G}{\partial a}(\tau^*,0,0,\varepsilon) = 2.$$

Now, we only need to find $\frac{\partial F}{\partial a}(\tau^*,0,0,\varepsilon)$ to finish the computation of the coefficient matrix of system (25). By taking the derivative of function F with respect to a,

$$\frac{\partial F}{\partial a}(\tau,a,b,\varepsilon) = \frac{\partial x^C}{\partial a}(\tau;\boldsymbol{\eta},\mathbf{p}_s^R). \tag{31}$$

In light of the first expression of (30), the evaluation in $(\tau^*,0,0,\varepsilon)$, lead us to

$$\frac{\partial F}{\partial a}(\tau^*,0,0,\varepsilon) = 2. \tag{32}$$

Let us now compute the second member of system (25). From the definition of function F, (see (13))

$$\frac{\partial F}{\partial b}(\tau,a,b,\varepsilon) = \frac{\partial x^C}{\partial b}(\tau;\boldsymbol{\eta},\mathbf{p}_s^R) + \frac{\varepsilon}{(1-b)^2}, \tag{33}$$

and then,

$$\frac{\partial F}{\partial b}(\tau^*,0,0,\varepsilon) = \frac{\partial x^C}{\partial b}(\tau^*;\mathbf{0},\mathbf{p}^*) + \varepsilon. \tag{34}$$

From the explicit expression of the solution in the central zone given in (16), we obtain

$$\begin{aligned} \frac{\partial x^C}{\partial b}(\tau^*;\mathbf{0},\mathbf{p}^*) &= -(\varepsilon\tau^*)/2, \\ \frac{\partial y^C}{\partial b}(\tau^*;\mathbf{0},\mathbf{p}^*) &= \varepsilon\left(1-\tau^*/2\right), \end{aligned} \tag{35}$$

and from the first expression here, we get

$$\frac{\partial F}{\partial b}(\tau^*,0,0,\varepsilon)=\varepsilon\,(1-\tau^*/2)\,. \tag{36}$$

Regarding $\frac{\partial G}{\partial b}(\tau^*,0,0,\varepsilon)$, from the definition of function G (see again (13)), we have

$$\frac{\partial G}{\partial b}(\tau,a,b,\varepsilon)=\frac{\partial y^C}{\partial b}(\tau;\boldsymbol{\eta},\mathbf{p}_s^R)+\frac{\varepsilon}{\lambda_s^L}\frac{\partial x^C}{\partial b}(\tau;\boldsymbol{\eta},\mathbf{p}_s^R). \tag{37}$$

From expressions in (35), we get

$$\frac{\partial G}{\partial b}(\tau^*,0,0,\varepsilon)=\varepsilon\,(1-\tau^*/2)\,, \tag{38}$$

which is the same as $\frac{\partial F}{\partial b}(\tau^*,0,0,\varepsilon)$.

Thus, we obtain that system (25) is equivalent to

$$\begin{pmatrix}\lambda_s^R\varepsilon & 2\\ 0 & 2\end{pmatrix}\begin{pmatrix}\dfrac{\partial\tilde{\tau}}{\partial b}(0,\varepsilon)\\ \dfrac{\partial\tilde{a}}{\partial b}(0,\varepsilon)\end{pmatrix}=\varepsilon\,(\tau^*/2-1)\begin{pmatrix}1\\1\end{pmatrix}.$$

When $\varepsilon\neq 0$, this system has a unique solution, which is given by

$$\frac{\partial\tilde{\tau}}{\partial b}(0,\varepsilon)=0 \quad\text{ and }\quad \frac{\partial\tilde{a}}{\partial b}(0,\varepsilon)=-\varepsilon\,(\tau^*/2-1)\,/2.$$

Analogously, the implicit differentiation of functions F and G up to order two allows us to obtain the second-order derivatives. This finishes the proof.

We use the approximation of $\tilde{a}(b,\varepsilon)$ obtained in this section to establish the stability of the corresponding canard cycles.

5.4. *Proof of Theorem 4.5*

Let us now focus on the stability of the family of canard cycles; see Fig. 8. First, we are going to measure how the orbits approach the slow manifolds μ_s^L and μ_s^R, in their respective zones. The intersection between the left slow manifold μ_s^L and the left separation line $x=-\varepsilon/(1-b):=x_0^L$ is given by $\mathbf{p}_s^L=(x_0^L,y_0^L)^T$, with $y_0^L=-a-\varepsilon+(\varepsilon/(1-b)+a)/\lambda_s^L$. Consider an orbit with initial point in the left straight separation line above the invariant manifold μ_s^L and below the line $y=-x$, that is, $\mathbf{p}_1=(x_0^L,y_0^L+\delta)^T$, with $\delta>0$ and small enough. At each time t, the distance between that orbit and the invariant manifold μ_s^L is given by

$$\mathbf{d}^L(t;\boldsymbol{\eta},\delta)=\alpha^L\exp(\lambda_s^Lt)\mathbf{v}_s^L+\beta^L\exp(\lambda_f^Lt)\mathbf{v}_f^L, \tag{39}$$

where

$$\mathbf{v}_s^L=\mathbf{p}_s^L-\mathbf{q}^L=\left(\frac{\varepsilon}{1-b}+a\right)\left(-1,\frac{\varepsilon}{\lambda_s^L}\right)^T \quad\text{ and }\quad \mathbf{v}_f^L=(-\lambda_f^L,\varepsilon)^T$$

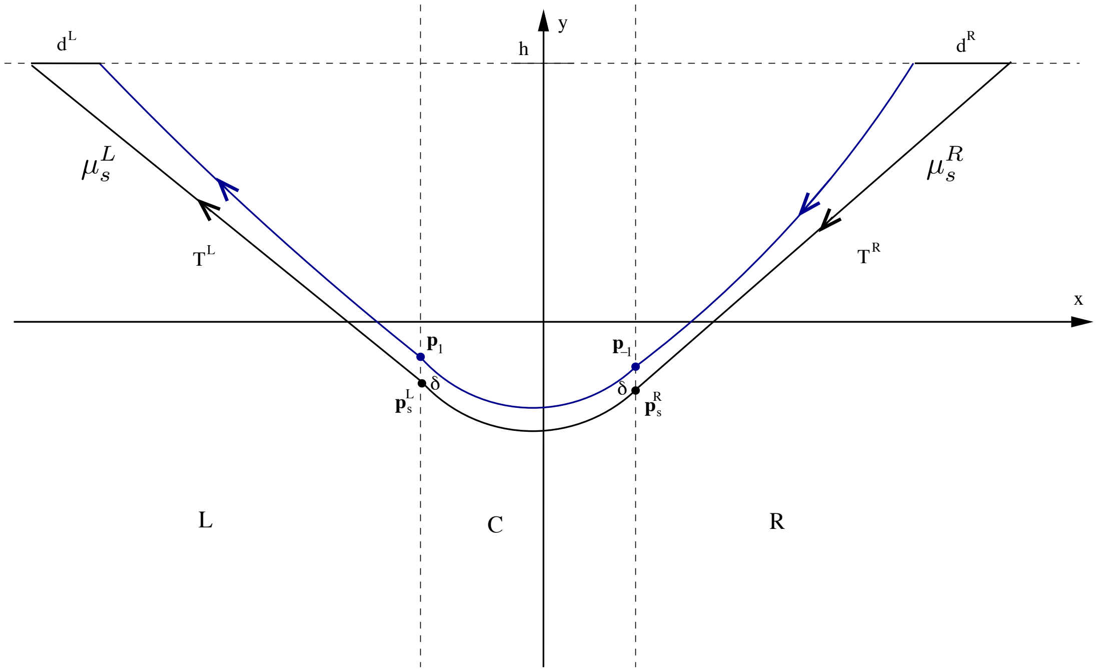

Figure 8. Sketch of the canard cycle (in black) and one orbit close to it (in blue) for the stable case $b > 0$.

are the eigenvectors corresponding to the eigenvalues λ_s^L, λ_f^L, and $\mathbf{q}^L$ is the virtual equilibrium point of the left zone. By imposing $\mathbf{d}^L(0; \boldsymbol{\eta}, \delta) = (0, \delta)^T$, one can compute

$$\alpha^L = -\frac{\beta^L \lambda_f^L}{\frac{\varepsilon}{1-b} + a}, \qquad \beta^L = \frac{\delta \lambda_s^L}{\varepsilon(\lambda_s^L - \lambda_f^L)}.$$

The intersection between the right slow manifold μ_s^R and the right separation line $x = \varepsilon/(1+b)$ is given by $\mathbf{p}_s^R$ in (9). Consider an orbit backwards in time with initial point in the right straight separation line above the invariant manifold μ_s^R and below the line $y = x$, that is, $\mathbf{p}_{-1} = (x_0^R, y_0^R + \delta)^T$, with $\delta > 0$ and small enough. At each time t, the distance between that orbit (backwards, localized in the right zone), and the invariant manifold μ_s^R is given by

$$\mathbf{d}^R(t; \boldsymbol{\eta}, \delta) = \alpha^R \exp(-\lambda_s^R t)\mathbf{v}_s^R + \beta^R \exp(-\lambda_f^R t)\mathbf{v}_f^R, \tag{40}$$

where

$$\mathbf{v}_s^R = \mathbf{p}_s^R - \mathbf{q}^R = \left(\frac{\varepsilon}{1+b} - a\right)\left(-1, \frac{\varepsilon}{\lambda_s^R}\right)^T \quad \text{and} \quad \mathbf{v}_f^R = (-\lambda_f^R, \varepsilon)^T$$

are the eigenvectors corresponding to the eigenvalues λ_s^R, λ_f^R, and $\mathbf{q}^R$ is the virtual equilibrium point of the right zone. By imposing $\mathbf{d}^R(0;\boldsymbol{\eta},\delta)=(0,\delta)^T$, we obtain

$$\alpha^R=\frac{\beta^R\lambda_f^R}{\frac{\varepsilon}{1+b}-a},\qquad \beta^R=\frac{\delta\lambda_s^R}{\varepsilon(\lambda_s^R-\lambda_f^R)}.$$

In functions (39) and (40), the contribution of the addend corresponding to the slow eigenvector can be neglected in comparison to that of the fast one. Moreover, as $\lambda_f^R=-\lambda_f^L$ and $\lambda_s^R=-\lambda_f^R$, we conclude that $\beta^L=\beta^R$. Thus, we can conclude that the stability is determined by the function

$$s(\boldsymbol{\eta})=\exp(\lambda_f^L(T^L-T^R)), \tag{41}$$

where T^L is the time that the orbit on the left slow manifold takes to arrive from the separation line of the left zone to a height h, and T^R is the time that the orbit on the right slow manifold takes to arrive from a height h to the separation line of the right zone. The limit cycle will be stable if $s(\boldsymbol{\eta})<1$ and unstable if $s(\boldsymbol{\eta})>1$. So, to know the stability, we only have to find the sign of T^L-T^R. Despite the apparent symmetry of the system, if $b\neq 0$, $T^L\neq T^R$ in every case, because the distance from the corresponding virtual equilibrium point to left and right boundaries is not equal (see Fig. 3). Times T^R and T^L depend mainly on this distance. Consider $b>0$. We know from Lemma 4.4 that the canard cycle exists for $a\simeq\frac{\pi}{4}\sqrt{\varepsilon}b>0$. Thus, the equilibrium point is located in $x>0$, closer to $x=\varepsilon/(1+b)$ and the orbit takes more time to arrive from h to the right boundary than from the left boundary to h because of the presence of the equilibrium point. That is, in this case $T^R>T^L$ and

$$s(\eta)<\exp(-c/\varepsilon),\quad \text{where } c \text{ is a positive constant independent of } \varepsilon. \tag{42}$$

Then, the orbit is stable. Analogous reasoning allow us to conclude that the orbit is unstable for $b<0$. Note that the passage through the middle zone does not play any role because of the estimate of the passage time given by τ^* in (8).

We compute explicitly the stability function $s(\boldsymbol{\eta})$ to confirm that the above intuitive reasoning is true. The explicit expressions of T^L and T^R are given by

$$T^L=\frac{1}{\lambda_s^L}\log\left(\frac{\lambda_s^L(h+\varepsilon+a)}{\varepsilon\left(\frac{\varepsilon}{1-b}+a\right)}\right) \tag{43}$$

and

$$T^R=\frac{1}{\lambda_s^L}\log\left(\frac{\lambda_s^L(h+\varepsilon-a)}{\varepsilon\left(\frac{\varepsilon}{1+b}-a\right)}\right). \tag{44}$$

It is easy to see that

$$s(\boldsymbol{\eta})=\left(\frac{(h+\varepsilon+a)\left(\frac{\varepsilon}{1+b}-a\right)}{(h+\varepsilon-a)\left(\frac{\varepsilon}{1-b}+a\right)}\right)^{\lambda_f^L/\lambda_s^L}. \tag{45}$$

Then we remark that

$$\lambda_f^L/\lambda_s^L \simeq 1/\varepsilon. \tag{46}$$

For the case of the existence of the canard cycle, we know from Lemma 4.4 that $a \simeq \frac{\pi}{4}\sqrt{\varepsilon}b$, or, if we consider $b = 2\hat{b}\sqrt{\varepsilon}$,

$$a \simeq \frac{\pi}{2}\varepsilon\hat{b}. \tag{47}$$

By construction of the system, we have that $a \in (-\varepsilon/(1-b), \varepsilon/(b+1))$, hence the following condition for $\hat{b}$ is satisfied

$$-2/\pi < \hat{b} < 2/\pi. \tag{48}$$

Considering approximation (47), we can write that

$$\frac{h+\varepsilon+a}{h+\varepsilon-a} \simeq 1 + \frac{\pi\varepsilon\hat{b}}{h} := 1/d(\hat{b}) \tag{49}$$

and that

$$\frac{\frac{\varepsilon}{1+b} - a}{\frac{\varepsilon}{1-b} + a} \simeq \frac{1 - \frac{\pi\hat{b}}{2}}{1 + \frac{\pi\hat{b}}{2}} := n(\hat{b}). \tag{50}$$

From expressions (46), (49) and (50), we conclude that (51) can be approximated by

$$s(\boldsymbol{\eta}) \simeq \left(\frac{n(\hat{b})}{d(\hat{b})}\right)^{1/\varepsilon}. \tag{51}$$

Taking into account (48), it comes that $n(\hat{b}), d(\hat{b}) > 0$. Moreover, $1/d(\hat{b}) = 1 + O(\varepsilon)$ and when $\hat{b} > 0$, $n(\hat{b}) < c_0 < 1$ for some constant c_0, so that $s(\boldsymbol{\eta})$ satisfies estimate (42) and therefore the orbit is stable. Finally, when $\hat{b} < 0$, $n(\hat{b}) > c_1 > 1$ for some constant c_1, so $s(\boldsymbol{\eta})$ is exponentially large and the orbit is unstable.

6. Conclusions and perspectives

In this paper, we have fully analyzed the generation mechanism giving rise to canard cycles in planar slow-fast PWL systems with three zones, that is, a connection between attracting and repelling slow manifolds and its break-up upon exponentially small parameter variation. We provide the first treatment of this problem from the viewpoint of Geometric Singular Perturbation Theory (GSPT), which allows a complete comparison with the smooth case and sets the basis for revisiting and hopefully simplifying GSPT by using the PWL framework.

We have proven the existence and stability of canard cycles due to the break-up of this connection and in a two-parameter unfolding. We focus on such cycles sufficiently close to the transition where they are created, that is, we only analyze canards without head.

A short-term objective is to add a third parameter (which we believe can control the slope of one branch of the critical manifold), in order to allow for the coexistence of a stable and an unstable canard cycle that would coalesce in a saddle-node bifurcation of limit cycles.

A second short-term objective is to analyze the global aspect of PWL canard cycles by adding a fourth zone mimicking the upper fold of the Van der Pol cubic critical manifold. It is known that this situation allows for PWL canards with head [36]. We plan to study the existence of such canard cycles using similar tools as in the present work.

A longer-term objective is to extend our results to 3D slow-fast PWL systems displaying canard phenomena. There are two main families of such systems, depending on whether the third variable is slow or fast; the overarching goal is to study complex oscillations due to multiple time scales in the framework of PWL systems. In the former case, we aim to study slow passage through canard explosion in a PWL context, as a fundamental step to prove the existence and patterns of Mixed-Mode Oscillations (MMOs) in PWL vector fields, following the construction provided in [11]. In the latter case, we plan to investigate spike-adding canard explosion [10] in the PWL framework.

References

[1] A. Andronov, A. Vitt and S. Khaikin, *Theory of oscillators*, Pergamon Press, Oxford, 1966.

[2] N. Arima, H. Okazaki and H. Nakano, *A generation mechanism of canards in a piecewise linear system*, IEICE T. Fundam. Electr. **80**(3): 447–453, 1997.

[3] E. Benoît, J.-L. Callot, F. Diener and M. Diener, *Chasse au Canard*, Collect. Math. **32**(1-2): 37–119, 1981.

[4] B. Braaksma, *Singular Hopf bifurcation in systems with fast and slow variables*, J. Nonlinear Sci. **8**(5): 457–490, 1998.

[5] M. Brøns, *Bifurcations and instabilities in the Greitzer model for compressor system surge*, Math. Eng. Ind. **2**(1): 51–63, 1988.

[6] M. Brøns, *Excitation and annihilation in the FitzHugh-Nagumo equations*, IMACS Trans. Sci. Comp. **1**(1): 297–301, 1989.

[7] M. Brøns and K. Bar-Eli, *Canard explosion and excitation in a model of the Belousov-Zhabotinsky reaction*, J. Phys. Chem. **95** 8706–8713, 1991.

[8] V. Carmona, E. Freire, E. Ponce and F. Torres, *The continuous matching of two stable linear systems can be unstable*, Discrete Contin. Dyn. Syst. **16**(3): 689–703, 2006.

[9] M. Desroches, E. Freire, S.J. Hogan, E. Ponce, and P. Thota, *Canards in piecewise-linear systems: explosions and super-explosions*, Proc. R. Soc. A. **469**(2154): 20120603, 2013.

[10] M. Desroches, T. J. Kaper and M. Krupa, *Mixed-mode bursting oscillations: Dynamics created by a slow passage through spike-adding canard explosion in a square-wave burster.* Chaos **23**(4): 046106, 2013.

[11] M. Desroches, E. Freire, A. Guillamon, R. Prohens, E. Ponce and A. E. Teruel, *Canards, folded nodes and mixed-mode oscillations in piecewise-linear systems.* Preprint, 2014.

[12] F. Dumortier and R. Roussarie, *Canard cycles and center manifolds.* Mem. Amer. Math. Soc. **121**(577) 1996.

[13] M. di Bernardo, C. J. Budd, A. R. Champneys and P. Kowalczyk, *Piecewise-smooth dynamical systems. Theory and applications*, Springer-Verlag London, London, 2008.

[14] W. Eckhaus, *Standard chase on French Ducks*, Lecture Notes in Math. **985** 449–494, 1983.

[15] N. Fenichel, *Persistence and smoothness of invariant manifolds for flows*, Indiana Univ. Math. J. **21**(3):193–226, 1971-1972.

[16] N. Fenichel, *Geometric singular perturbation theory for ordinary differential equations*, J. Differential Equations **31**(1):53–98, 1979.

[17] R. FitzHugh, *Impulses and physiological states in theoretical models of nerve membrane*, Biophys. J. **1**(6): 445–466, 1961.

[18] E. Freire, E. Gamero and A. J. Rodríguez-Luis, *First-order approximation for canard periodic orbits in a Van der Pol electronic oscillator*, Appl. Math. Lett. **12**(2): 73–78, 1999.

[19] E. Freire, E. Ponce, F. Rodrigo and F. Torres, *Bifurcation sets of continuous piecewise linear systems with two zones*, Internat. J. Bifur. Chaos Appl. Sci. Engrg. **8**(11): 2073–2097, 1998.

[20] E. Freire, E. Ponce and F. Torres, *Hopf-like bifurcations in planar piecewise linear systems*, Publ. Mat. **41**(1): 135–148, 1997.

[21] J. Guckenheimer, *Singular Hopf bifurcation in systems with two slow variables*, SIAM J. Appl. Dyn. Syst. **7**(4): 1355–1377, 2008.

[22] E. M. Izhikevich, *Synchronization of elliptic bursters*, SIAM Rev. **43**(2): 315–344, 2001.

[23] M. Komuro and T. Saito, *"Lost solution" in a piecewise linear system*, IEICE T. Fundam. Electr. **74**(11): 3625–3627, 1991.

[24] G. A. Kriegsmann, *The rapid bifurcation of the Wien bridge oscillator*, IEEE Trans. Circuits Syst. **34**(9): 1093–1096, 1987.

[25] M. Krupa and P. Szmolyan, *Extending geometric singular perturbation theory to nonhyperbolic points-fold and canard points in two dimensions*, SIAM J. Math. Anal. **33**(2): 286–314, 2001.

[26] M. Krupa and P. Szmolyan, *Relaxation oscillation and canard explosion*, J. Differential Equations **174**(2): 312–368, 2001.

[27] M. Krupa, N. Popovic, N. Kopell, and H. G. Rotstein, *Mixed-mode oscillations in a three time-scale model for the dopaminergic neuron*, Chaos **18**(1): 015106, 2008.

[28] M. Kunze, Non-smooth dynamical systems, Lecture Notes in Mathematics Vol.**1744**, Springer, 2000.

[29] G. M. Maggio, M. di Bernardo and M. P. Kennedy., *Nonsmooth bifurcations in a piecewise linear model of the Colpitts oscillator*, IEEE Trans. Circuits Systems **47**(8):1160–1177, 2000.

[30] A. I. Mees and L. O. Chua, *The Hopf bifurcation theorem and its applications to nonlinear oscillations in circuits and systems*, IEEE Trans. Circuits Syst. **26**(4): 235–254, 1979.

[31] J. Moehlis, *Canards for a reduction of the Hodgkin-Huxley equations*, J. Math. Biol. **52**(2): 141–153, 2006.

[32] J. Nagumo, S. Arimoto and S. Yoshizawa, *An active pulse transmission line simulating nerve axon*, Proc. IRE **50**(10): 2061–2070, 1962.

[33] R. Prohens and A. E. Teruel, *Canard trajectories in 3d piecewise linear systems*, Discrete Contin. Dyn. Syst. **33**: 4595–4611, 2013.

[34] R. Prohens, A. E. Teruel, and C. Vich, *Slow-fast n-dimensional piecewise-linear differential systems.* Preprint, 2014.

[35] D. J. W. Simpson and R. Kuske, *Mixed-mode oscillations in a stochastic, piecewise-linear system*, Phys. D **240**(14): 1189–1198, 2011.

[36] H. G. Rotstein, S. Coombes and A. M. Gheorghe, *Canard-like explosion of limit cycles in two-dimensional piecewise-linear models of FitzHugh-Nagumo type*, SIAM J. Appl. Dyn. Syst. **11**(1): 135–180, 2012.

[37] C.W. Wu, L. Pivka and A. Huang, *Lorenz equation and Chua's equation*, Internat. J. Bifur. Chaos Appl. Sci. Engrg. **6**(12b): 2443–2489, 1996.